Detector-Level Performance Limits of FSOC Systems Over Málaga Atmospheric Turbulence: A Comparative Study of PIN, APD and SPD Technologies

Original research

Received: XX December 20XX
Accepted: XX December 20XX
Online Ready: XX December 20XX

Abstract

Free-Space Optical Communication (FSO) has emerged as a promising solution for next-generation wireless networks, offering ultra-high bandwidth, security, scalability and interference-free transmission. However, its performance remains highly sensitive to atmospheric turbulence and photodetector characteristics. This paper presents a unified analytical and numerical framework for evaluating the performance of three major photodetectors namely Positive-Intrinsic-Negative (PIN) photodetectors, Avalanche Photodiode (APD), and Single-Photon Detector (SPD) under Málaga-distributed turbulence, a generalized model encompassing weak to strong scintillation regimes. Unlike other turbulence models that are limited to a specific scenario, the Málaga distribution is evolutionary, capturing a wide range of realistic and dynamically varying atmospheric conditions, which provides a more comprehensive and practical basis for assessing FSOC system performance. The formulation integrates geometric and atmospheric attenuation, turbulence-induced irradiance fluctuations, and detector-specific gain and noise mechanisms to assess key performance metrics including Signal-to-Noise Ratio, Symbol Error Rate, noise variance, dynamic range, and linearity. Simulation results show that the SPD achieves the highest sensitivity and longest range, maintaining an SNR of 15 dB and an SER near 10^{-6} up to 50-55 km, followed by the APD (≈30 km) and PIN (≈25 km). The PIN exhibits the lowest noise (10^{-10} A) and widest dynamic range (70 dB), whereas the APD provides the most stable linearity. These findings align with and extend existing literature by combining Málaga turbulence modeling with detector-level physical analysis and Monte Carlo validation. The results establish clear operational domains for each detector type and provide a practical foundation for the design of robust, high-performance FSOC systems resilient to atmospheric impairments.

Keywords: Avalanche Photodiode; FSOC; Málaga distribution; Positive-Intrinsic-Negative photodetector;

1 Introduction

Optical communication systems have gained remarkable attention in recent years, driven by rapid advances in Free-Space Optical Communication (FSOC) technologies. FSOC offers several advantages over conventional wired and wireless communication systems, notably its exceptionally high bandwidth, immunity to electromagnetic interference, and license-free operation (1). Unlike traditional radio-frequency (RF) communication, which requires spectrum allocation and suffers from interference and congestion, FSOC employs narrow optical beams to transmit information through the atmosphere, achieving higher data rates, enhanced security, and reduced latency (1; 2). Fundamentally, FSOC systems rely on modulated light waves to encode and transmit digital information, eliminating the need for physical cables or optical fibers (2). This property makes FSOC inherently flexible, cost-effective, and rapidly deployable, positioning it as a key enabler for last-mile connectivity, backhaul links, and temporary high-capacity links in emergency or remote areas. Owing to these unique features, FSOC has attracted increasing interest from both the academic community and the telecommunications industry. Recent developments have extended FSOC applications into next-generation mobile communication networks (5G and beyond) and Unmanned Aerial Vehicle (UAV) platforms (3). These emerging use cases demand high-capacity, low-latency, and interference-free links, all of which FSOC can deliver under favorable atmospheric conditions. Nevertheless, atmospheric impairments such as fog, rain, turbulence, and misalignment remain major challenges, as they introduce signal attenuation and fluctuations that degrade system performance.

At the heart of every FSOC receiver lies a photodetector, a critical component responsible for converting incident optical power into electrical current (4). The selection of an appropriate photodetector has a profound impact on system performance, as it determines the overall responsivity, sensitivity, noise behavior, bandwidth, and detection accuracy (4; 5). In recent years, researchers have explored various receiver architectures and photodetection technologies to improve detection sensitivity and minimize bit error rates (BER). Among these, the PIN photodiode has been widely used due to its linearity, low dark current, and broad bandwidth, making it well-suited for short- and medium-range FSOC links operating under moderate turbulence conditions (6). Conversely, the Avalanche Photodiode (APD) has gained prominence for its internal avalanche gain, which amplifies weak optical signals and enhances sensitivity, albeit at the cost of increased excess noise that must be optimized through careful design (6; 7). More recently, Single-Photon Detectors (SPDs) encompassing Geiger-mode APDs and Superconducting Nanowire Single-Photon Detectors (SNSPDs) have demonstrated the capability to detect individual photons, enabling ultra-sensitive detection for quantum communication, deep-space optical links, and ultra-long-range FSOC systems (8). These detectors mark a major leap in optical receiver technology, opening new avenues for communication in extreme low-light and high-turbulence environments.

In parallel, a substantial body of research has focused on improving the reliability and robustness of FSOC links under adverse atmospheric conditions. Early theoretical works primarily centered on channel modeling to describe turbulence-induced irradiance fluctuations using statistical distributions such as log-normal, K-distribution, and Gamma-Gamma models (9; 10). Although these models accurately capture certain turbulence regimes, they often fail to provide consistent performance predictions across the full range of atmospheric conditions. To overcome this limitation, the Málaga ($\mathcal{M}$) distribution was introduced as a generalized statistical framework capable of modeling both weak and strong turbulence, subsuming the aforementioned models as special cases (10; 11). This comprehensive model provides a more realistic characterization of optical channel fading and is therefore widely adopted in modern FSOC performance evaluations. In this context, the design and selection of photodetectors emerge as critical factors in mitigating turbulence-induced signal

degradation. Indeed, even when the propagation channel is well characterized, overall link reliability ultimately depends on the detector's ability to convert distorted optical signals into accurate electrical representations. Therefore, understanding the operational principles, responsivity, and noise characteristics of various photodetectors becomes indispensable for optimizing FSOC receiver design under realistic atmospheric conditions.

Building on these considerations, this study aims to perform a comparative performance analysis of PIN, APD, and SPD photodetectors operating over Málaga turbulence channels in Côte d'Ivoire subtropical environnement. Through the evaluation of key performance indicators such as linearity, dynamic range, noise variance, and symbol error rate (SER), this work seeks to provide comprehensive insights into the trade-offs and optimal configurations of photodetectors for achieving robust, energy-efficient, and high-performance FSOC systems in turbulent environments.

2 Theoretical Analysis

2.1 Beam Spot and Geometric Loss

In a typical FSOC system, the optical beam emitted by the transmitter propagates through the atmosphere and gradually diverges due to diffraction and beam spreading effects (4; 12). Assuming a Gaussian beam profile, the radius of the optical spot at the receiver plane can be approximated as the product of the beam divergence half-angle θ and the propagation distance L. Accordingly, the spot area at the receiver is given by (12):

$$A_{\text{spot}} = \pi(\theta L)^2. \tag{1}$$

This quadratic dependence on the distance illustrates that the optical footprint expands rapidly as the link length increases, thereby reducing the optical power density at the receiver.

The fraction of the transmitted power effectively collected by the receiver is determined by the geometric loss factor G_{geo}, defined as the ratio between the receiver's effective aperture area A_{eff} and the total beam spot area A_{spot} (13):

$$G_{\text{geo}} = \frac{A_{\text{eff}}}{A_{\text{spot}}} = \frac{A_{\text{eff}}}{\pi(\theta L)^2}. \tag{2}$$

This factor quantifies the geometrical coupling efficiency of the system, accounting for both beam divergence and pointing misalignment. As the link distance increases or the divergence angle widens, G_{geo} decreases significantly, leading to higher geometric attenuation.

In practice, however, FSOC links are also subject to atmospheric attenuation, primarily caused by molecular absorption, aerosol scattering, and hydrometeoric effects such as fog, haze, or rain. These effects introduce an exponential loss along the propagation path, modeled by the Beer-Lambert law (14):

$$G_{\text{atm}} = \exp(-\alpha L), \tag{3}$$

where α (in dB/km or km^{-1}) denotes the atmospheric attenuation coefficient, which depends on wavelength, visibility, and weather conditions.

Combining the geometric and atmospheric effects, the deterministic received optical power in the absence of turbulence is expressed as (13; 14):

$$P_r^{(0)} = P_t G_{\text{geo}} G_{\text{atm}}, \tag{4}$$

where P_t is the transmitted optical power. This expression defines the baseline received power governed solely by deterministic propagation losses.

In realistic FSOC environments, atmospheric turbulence introduces additional stochastic fluctuations in the received optical intensity due to random refractive index variations along the optical path (12; 14). These fluctuations cause scintillation, beam wander, and intensity fading, which are often

modeled using statistical distributions. While classical models such as log-normal, K-distribution, and Gamma-Gamma distributions are valid in limited turbulence regimes, they fail to accurately describe the complete range of turbulence conditions encountered in practical FSOC links (11). To overcome this limitation, the Málaga ($\mathcal{M}$) distribution was proposed as a generalized turbulence model capable of encompassing both weak and strong turbulence scenarios as well as the effects of line-of-sight (LOS) and non-line-of-sight (NLOS) components. The probability density function (PDF) of the normalized irradiance I under Málaga turbulence is given by (11; 15):

$$f_I(I) = A \sum_{m=1}^{\beta} a_m I^{\frac{\alpha+m}{2}-1} K_{\alpha-m}\left(2\sqrt{\frac{\alpha\beta I}{g\beta+\Omega'}}\right), \tag{5}$$

where:

- α represents the effective number of large-scale turbulent eddies,
- β characterizes the number of small-scale turbulent cells,
- g is the average power of the scattered components,
- Ω' denotes the average power of the LOS component,
- $K_\nu(\cdot)$ is the modified Bessel function of the second kind,
- and A and a_m are normalization constants defined as (11; 15):

$$A = \frac{2\alpha^{\frac{\alpha}{2}}}{g^{1+\frac{\alpha}{2}}\Gamma(\alpha)}\left(\frac{g\beta}{g\beta+\Omega'}\right)^{\beta+\frac{\alpha}{2}}, \tag{6}$$

$$a_m = \binom{\beta-1}{m-1}\frac{(g\beta+\Omega')^{1-\frac{m}{2}}}{(m-1)}\left(\frac{\Omega'}{g}\right)^{m-1}. \tag{7}$$

This expression reduces to the Gamma-Gamma and K-distribution models for specific parameter choices, making it one of the most versatile turbulence models for FSOC system analysis.

Incorporating the effects of atmospheric attenuation, geometric spreading, and turbulence, the instantaneous received optical power can be expressed as (9; 12):

$$P_r = P_t G_{\text{geo}} G_{\text{atm}} I. \tag{8}$$

The stochastic behavior of I dominates the link performance and directly impacts key metrics such as the Signal-to-Noise Ratio, Bit Error Rate, and Symbol Error Rate. At the receiver, the photodetector converts the incoming optical power into an electrical current according to its responsivity R (A/W). The corresponding mean photocurrent is therefore given by (15; 16):

$$\bar{i} = RP_r = RP_t G_{\text{geo}} G_{\text{atm}} I. \tag{9}$$

This relationship clearly indicates that the output current depends jointly on the transmitter power, link geometry, atmospheric attenuation, turbulence fluctuations, and detector responsivity. However, the photodetection process is inevitably affected by multiple noise sources that degrade the received electrical signal. The total noise variance, denoted as σ^2_{noise}, can be modeled as the sum of statistically independent noise components (17; 18):

$$\sigma^2_{\text{noise}} = \sigma^2_{\text{shot}} + \sigma^2_{\text{thermal}} + \sigma^2_{\text{amp}}, \tag{10}$$

where σ^2_{shot} accounts for quantum (shot) noise due to the discrete nature of photon arrivals, $\sigma^2_{\text{thermal}}$ represents thermal (Johnson–Nyquist) noise generated in the receiver circuitry, and σ^2_{amp} denotes amplifier noise from post-detection electronics.

Among these, shot noise and thermal noise typically dominate in FSOC systems. The shot noise variance is mathematically expressed as (18):

$$\sigma^2_{\text{shot}} = 2q(\bar{i} + I_{\text{bg}})B, \tag{11}$$

where q is the elementary charge, B is the receiver bandwidth, and I_{bg} is the background-light-induced current. This expression emphasizes that the shot noise power scales with both the signal level and the ambient background, underlining the importance of optical filtering, receiver shielding, and bandwidth optimization for achieving high SNR in FSOC links.

2.2 Signal-to-Noise Ratio (SNR) Models

The Signal-to-Noise Ratio is a fundamental performance metric for evaluating the quality of optical signal reception in FSOC systems. It quantifies the ratio between the useful photocurrent power and the total noise power at the receiver, thus reflecting the reliability of data detection under various atmospheric conditions (1). Considering both deterministic attenuation mechanisms (geometric loss and atmospheric absorption) and stochastic fading effects (turbulence-induced scintillation), the instantaneous received optical power at the detector input can be expressed, as defined in Equation (8). The corresponding instantaneous SNR at the receiver can then be written as (17; 18):

$$\text{SNR}(I) = \frac{\bar{i}^2}{\sigma^2_{\text{noise}}}, \tag{12}$$

where $\bar{i}$ denotes the mean photocurrent, and σ^2_{noise} represents the total noise variance encompassing all major noise components (shot noise, thermal noise, amplifier noise, and background-induced fluctuations).

- PIN Photodiode :
  the PIN photodiode operates without internal gain and provides a linear response with relatively low dark current, making it well suited for short-to-medium range FSOC links. The total noise variance in a PIN-based receiver is dominated by shot noise and thermal noise, and can be expressed as (17; 19):

$$\sigma^2_{\text{PIN}} = 2q(\bar{i} + I_{\text{bg}})B + \frac{4kTB}{R_L}, \tag{13}$$

  where q is the electron charge, B the receiver bandwidth, I_{bg} the background-induced current, k Boltzmann's constant, T the receiver temperature, and R_L the load resistance.
  Substituting $\bar{i} = RP_tG_{\text{geo}}G_{\text{atm}}I$ into the above expression yields the instantaneous SNR for the PIN receiver:

$$\text{SNR}_{\text{PIN}}(I) = \frac{(RP_tG_{\text{geo}}G_{\text{atm}}I)^2}{2q\left(RP_tG_{\text{geo}}G_{\text{atm}}I + I_{\text{bg}}\right)B + \frac{4kTB}{R_L}}. \tag{14}$$

  To account for turbulence-induced irradiance fluctuations, the average SNR over Málaga turbulence is obtained by statistical averaging using the irradiance PDF $f_I(I)$:

$$\overline{\text{SNR}}_{\text{PIN}} = \int_0^\infty \text{SNR}_{\text{PIN}}(I) f_I(I) dI. \tag{15}$$

  This formulation links the detector response directly to the turbulence strength and atmospheric attenuation parameters.

- Avalanche Photodiode (APD) :
  The Avalanche Photodiode (APD) introduces an internal gain M through the avalanche multiplication process, thereby enhancing weak-signal detection. However, this gain also amplifies the noise, particularly shot noise, which is scaled by the excess noise factor $F(M)$. The total noise variance for an APD receiver is given by (17; 20):

$$\sigma^2_{\text{APD}} = 2qM^2(\bar{i} + I_{\text{bg}})BF(M) + \frac{4kTB}{R_L}, \tag{16}$$

where the excess noise factor is typically modeled as (20):

$$F(M) = kM + (1-k)\left(2 - \frac{1}{M}\right), \tag{17}$$

and k is the ionization coefficient ratio (ranging from 0.02 to 0.3 depending on the detector material).

The instantaneous SNR for the APD under Málaga turbulence is then:

$$\mathrm{SNR}_{\mathrm{APD}}(I) = \frac{(MRP_tG\mathrm{geo}G_{\mathrm{atm}}I)^2}{2qM^2(RP_tG_{\mathrm{geo}}G_{\mathrm{atm}}I + I_{\mathrm{bg}})BF(M) + \frac{4kTB}{R_L}}. \tag{18}$$

The average SNR is obtained by integrating over the Málaga irradiance distribution:

$$\overline{\mathrm{SNR}}_{\mathrm{APD}} = \int_0^\infty \mathrm{SNR}_{\mathrm{APD}}(I) f_I(I) dI. \tag{19}$$

This comprehensive formulation enables simultaneous evaluation of the effects of turbulence, atmospheric losses, detector gain, and excess noise, thereby allowing accurate performance prediction under diverse FSOC channel conditions.

- Single-Photon Detector (SPD) :
  The Single-Photon Detector (SPD) operates in the photon-counting regime, where each detected photon corresponds to a discrete electrical event. The number of detected photons N during an observation interval follows Poisson statistics with a mean value $\lambda = \eta P_r/(h\nu)$, where η is the detector quantum efficiency, h Planck's constant, and ν the optical frequency. The corresponding variance is $\sigma_N^2 = N = \lambda$.

  Accordingly, the instantaneous SNR for the SPD under Málaga turbulence can be approximated as (21):

$$\mathrm{SNR}_{\mathrm{SPD}}(I) = \frac{N^2}{\sigma_N^2 + N_d + N_b} \approx \frac{N}{1 + \frac{N_d + N_b}{N}}, \tag{20}$$

  where N_d and N_b denote the dark count rate and background photon count, respectively. Since N is proportional to the received power $P_r = P_tG\mathrm{geo}G_{\mathrm{atm}}I$, the SNR scales linearly with turbulence-affected irradiance:

$$\mathrm{SNRSPD}(I) \propto P_tG\mathrm{geo}G_{\mathrm{atm}}I. \tag{21}$$

  The average SNR of the SPD is finally obtained by averaging over the Málaga-distributed irradiance:

$$\overline{\mathrm{SNR}}_{\mathrm{SPD}} = \int_0^\infty \mathrm{SNR}_{\mathrm{SPD}}(I) f_I(I) dI. \tag{22}$$

  This unified SNR framework underscores the interplay between optical attenuation mechanisms (G_{geo}, G_{atm}), turbulence-induced fading (I modeled by the Málaga PDF), and detector-specific parameters (R, M, $F(M)$, η).

  Overall, this analytical framework provides a comprehensive foundation for modeling and predicting FSOC link performance under realistic atmospheric conditions. It enables the optimization of photodetection architectures and the selection of suitable detectors according to link distance, channel turbulence, and operational wavelength.

3 Symbol Error Rate under Málaga Turbulence

In Free-Space Optical Communication systems employing intensity modulation and direct detection (IM/DD), the Symbol Error Rate serves as a critical metric for quantifying system

reliability. It represents the probability that a transmitted optical symbol is incorrectly detected due to the combined effects of thermal noise, shot noise, and turbulence-induced irradiance fluctuations. For a given instantaneous Signal-to-Noise Ratio SNR(I), the conditional SER of a binary modulation scheme such as On-Off Keying (OOK) can be expressed as (22):

$$\mathrm{SER}(\mathrm{SNR}(I)) = Q\left(\sqrt{\frac{\mathrm{SNR}(I)}{2}}\right), \tag{23}$$

where $Q(x) = \frac{1}{\sqrt{2\pi}} \int_x^\infty e^{-t^2/2} dt$ denotes the Gaussian Q-function. This expression reflects the instantaneous probability of symbol misdetection given a particular realization of the received irradiance I.

To incorporate the effects of atmospheric turbulence, the average SER is obtained by statistically averaging the conditional error probability over the distribution of I. Considering the Málaga (M) turbulence model, the average SER can be written as:

$$\overline{\mathrm{SER}} = \int_0^\infty \mathrm{SER}(\mathrm{SNR}(I)) f_I(I, \alpha, \beta, \Omega', g) dI, \tag{24}$$

where $f_I(\cdot)$ is the Málaga irradiance probability density function, and the parameters α, β, Ω', and g describe the large and small-scale turbulence strengths, the power of the line-of-sight component, and the scattered power contribution, respectively.

Given the nonlinear nature of the Q-function and the complex structure of the Málaga PDF, a closed-form analytical evaluation of this integral is generally intractable. Therefore, numerical integration or Monte Carlo simulations are typically employed to estimate the average SER with high precision.

3.1 Approximate Analytical Representation

For moderate-to-high SNR regimes, the Gaussian Q-function can be approximated using the exponential form (22; 23):

$$Q(x) \approx \frac{1}{2} e^{-x^2/2}, \tag{25}$$

which leads to an approximate expression for the conditional SER:

$$\mathrm{SER}(\mathrm{SNR}(I)) \approx \frac{1}{2} \exp\left(-\frac{\mathrm{SNR}(I)}{4}\right). \tag{26}$$

Substituting this into the average expression yields:

$$\overline{\mathrm{SER}} \approx \frac{1}{2} \int_0^\infty \exp\left(-\frac{\mathrm{SNR}(I)}{4}\right) f_I(I; \alpha, \beta, \Omega', g), dI. \tag{27}$$

Since SNR(I) depends linearly on I through the received power $P_r = P_t G_{\mathrm{geo}} G_{\mathrm{atm}} I$, the argument of the exponential reflects the fading-induced random variations in the instantaneous optical power.

3.2 Closed-Form Symbol Error Rate under Málaga Turbulence

Assuming a shot-noise or photon-limited regime, the instantaneous SNR varies linearly with the received irradiance I, i.e.,

$$\mathrm{SNR}(I) = \gamma I, \tag{28}$$

where γ is a detector-dependent scaling coefficient encompassing link and receiver parameters.

Under this assumption, the average SER over Málaga turbulence can be expressed as the Laplace transform (moment-generating function) of the irradiance PDF evaluated at $s = \gamma/4$ (11; 24):

$$\overline{\mathrm{SER}} \approx \frac{1}{2}\mathcal{L}_I(s)\big|_{s=\gamma/4} = \frac{1}{2}\, M_I\left(\frac{\gamma}{4}\right), \tag{29}$$

where $\mathcal{L}_I(s) = \mathbb{E}[e^{-sI}]$ and $M_I(\cdot)$ denote the Laplace transform and the MGF of the Málaga distribution, respectively.

The Laplace transform of the irradiance PDF under the Málaga ($\mathcal{M}$) turbulence model is given by (11; 24):

$$\mathcal{L}_I(s) = A \sum_{m=1}^{\beta} a_m\, 2\left(\frac{\alpha\beta}{g\beta+\Omega'}\right)^{\frac{\alpha+m}{4}} s^{-\frac{\alpha+m}{4}} K_{\alpha-m}\left(2\sqrt{\frac{\alpha\beta s}{g\beta+\Omega'}}\right), \tag{30}$$

where $K_\nu(\cdot)$ is the modified Bessel function of the second kind, and the parameters A and a_m are defined as equations (6) and (7).

Substituting $s = \gamma/4$ in (30), the average SER can be expressed in closed form as:

$$\overline{\mathrm{SER}} \approx A \sum_{m=1}^{\beta} a_m \left(\frac{\alpha\beta}{g\beta+\Omega'}\right)^{\frac{\alpha+m}{4}} \left(\frac{\gamma}{4}\right)^{-\frac{\alpha+m}{4}} K_{\alpha-m}\left(2\sqrt{\frac{\alpha\beta\gamma}{4(g\beta+\Omega')}}\right). \tag{31}$$

This unified expression links the Málaga channel parameters $(\alpha, \beta, \Omega', g)$ and the detector-dependent factor γ, allowing for direct SER prediction across receiver types.

3.3 Detector-dependent Coefficients

The linear SNR coefficients γ for each photodetector are expressed as follows (17; 19):

1) PIN Photodiode:

$$\gamma_{\mathrm{PIN}} = \frac{R\, P_t\, G_{\mathrm{geo}}\, G_{\mathrm{atm}}}{2qB}, \tag{32}$$

where R is the responsivity, B the electrical bandwidth, and q the electron charge.

Substituting $\gamma = \gamma_{\mathrm{PIN}}$ into (31) gives (17; 19):

$$\overline{\mathrm{SER}}_{\mathrm{PIN}} \approx A \sum_{m=1}^{\beta} a_m \left(\frac{\alpha\beta}{g\beta+\Omega'}\right)^{\frac{\alpha+m}{4}} \left(\frac{\gamma_{\mathrm{PIN}}}{4}\right)^{-\frac{\alpha+m}{4}} K_{\alpha-m}\left(2\sqrt{\frac{\alpha\beta\gamma_{\mathrm{PIN}}}{4(g\beta+\Omega')}}\right). \tag{33}$$

2) Avalanche Photodiode : including the excess noise factor $F(M)$, the coefficient becomes (6; 19):

$$\gamma_{\mathrm{APD}} = \frac{RP_tG_{\mathrm{geo}}G_{\mathrm{atm}}}{2qBF(M)}, \quad F(M) = kM + (1-k)\left(2 - \frac{1}{M}\right), \tag{34}$$

where M is the avalanche gain and k the ionization coefficient ratio.

The corresponding SER is:

$$\overline{\mathrm{SER}}_{\mathrm{APD}} \approx A \sum_{m=1}^{\beta} a_m \left(\frac{\alpha\beta}{g\beta+\Omega'}\right)^{\frac{\alpha+m}{4}} \left(\frac{\gamma_{\mathrm{APD}}}{4}\right)^{-\frac{\alpha+m}{4}} K_{\alpha-m}\left(2\sqrt{\frac{\alpha\beta\gamma_{\mathrm{APD}}}{4(g\beta+\Omega')}}\right). \tag{35}$$

3) Single-Photon Detector : for a photon-counting detector with mean photon arrival rate $N = \eta P_r T_s/(h\nu)$, the equivalent linear SNR coefficient is (25):

$$\gamma_{\mathrm{SPD}} = \frac{\eta\, P_t\, G_{\mathrm{geo}}\, G_{\mathrm{atm}}\, T_s}{h\nu}, \tag{36}$$

where η is the quantum efficiency, $h\nu$ the photon energy, and T_s the symbol duration. The resulting closed-form SER expression is:

$$\overline{\mathrm{SER}}_{\mathrm{SPD}} \approx A \sum_{m=1}^{\beta} a_m \left(\frac{\alpha\beta}{g\beta+\Omega'}\right)^{\frac{\alpha+m}{4}} \left(\frac{\gamma_{\mathrm{SPD}}}{4}\right)^{-\frac{\alpha+m}{4}} K_{\alpha-m}\left(2\sqrt{\frac{\alpha\beta\gamma_{\mathrm{SPD}}}{4(g\beta+\Omega')}}\right). \tag{37}$$

These results provide an analytical foundation for the optimization of FSOC receiver design under realistic Málaga turbulence conditions.

To complement the analytical derivations and assess their validity under practical conditions, Monte Carlo simulations were performed to numerically estimate the average SER under Málaga turbulence. This stochastic approach provides an efficient means of evaluating the influence of random irradiance fluctuations and detector characteristics on FSOC link performance, particularly in scenarios where closed-form analytical solutions are either intractable or computationally expensive.

4 Numerical simulation and Discussions

4.1 Numerical simulation configuration

In the simulation procedure, a large ensemble of irradiance samples I is first generated according to the Málaga probability density function, which accurately models the joint effects of small-scale and large-scale turbulence. Each generated sample represents a possible realization of the received optical intensity after propagation through a randomly perturbed atmospheric channel. For every irradiance realization, the instantaneous Signal-to-Noise Ratio, SNR(I), is computed using the corresponding expressions established in Section 3 for each photodetector type. These formulations inherently incorporate geometric and atmospheric attenuation (G_{geo}, G_{atm}) as well as detector-specific gain and noise parameters, ensuring realistic performance estimation. Once the instantaneous SNR values are obtained, the conditional Symbol Error Rate associated with each realization is evaluated using the Gaussian Q-function. The average SER is then estimated by averaging the conditional results over all realizations of I. The total number of Monte Carlo samples is ranging from 10^5 to 10^7 for statistical convergence. This simulation-based methodology offers several advantages. It not only enables direct numerical validation of the analytical expressions derived from the Málaga model but also provides a benchmark for performance evaluation under generalized turbulence scenarios, including extreme fading and strong scintillation. Moreover, the Monte Carlo framework can be extended to incorporate additional physical effects such as pointing errors, background illumination, and temporal beam wander, thereby yielding more comprehensive and realistic predictions of FSOC system behavior. By systematically varying the turbulence parameters $(\alpha, \beta, \Omega', g)$, the atmospheric attenuation coefficient, and the link distance L, one can assess the relative performance of PIN, APD, and SPD receivers under diverse operational conditions, thus guiding the optimal design of robust optical wireless communication systems.

The simulation parameters used in this study correspond to a typical free-space optical communication link operating at a wavelength of 1550 nm. The main physical constants include the electron charge $q = 1.602 \times 10^{-19}$ C, Planck's constant $h = 6.626 \times 10^{-34}$ J · s, and the speed of light $c = 3 \times 10^8$ m/s. The photon energy is computed as $h\nu = h\, c/\lambda$. The

transmitted optical power is set to $P_t = 0.1\,\mathrm{W}$, while atmospheric attenuation is modeled by an exponential decay term with a coefficient of $\alpha_{\mathrm{atm}} = 2 \times 10^{-4}\,\mathrm{m}^{-1}$. The optical beam exhibits a divergence angle of $\theta_{\mathrm{tx}} = 1\,\mathrm{mrad}$, and the receiver aperture has a diameter of $D_r = 0.10\,\mathrm{m}$, corresponding to an effective area $A_r = \pi D_r^2/4$. The link distance varies between 1 km and 100 km. For the PIN detector, the responsivity is $R = 0.8\,\mathrm{A/W}$, and the electrical bandwidth is $B_{\mathrm{el}} = 1\,\mathrm{GHz}$. The APD model incorporates an avalanche gain of $M_{\mathrm{APD}} = 10$ and an excess noise factor $F_{\mathrm{APD}} = 2$. The SPD is characterized by a photon detection efficiency of $\eta_{\mathrm{SPD}} = 0.7$, a detection time window $T_s = 1\,\mu\mathrm{s}$, a dark count rate of $\mathrm{DCR} = 100\,\mathrm{counts/s}$, and a leakage fraction $\varepsilon_{\mathrm{leak}} = 0.01$.

All analyses are performed over propagation distances ranging from 1 km to 100 km with 1 km increments. For each distance, the received signal power, signal-to-noise ratio, symbol error rate, noise RMS, dynamic range, and linearity are computed for the three detection technologies. These parameters are plotted as functions of distance to illustrate the performance evolution and to highlight the trade-offs between sensitivity, dynamic range, and proportional response across the different photodetectors.

4.2 Results

This section analyzes the simulation outcomes obtained for the Free-Space Optical Communication link under Málaga turbulence, focusing on five key performance metrics. Each metric serves a distinct purpose in evaluating the optical link's performance and helps characterize the relative advantages of the three photodetectors technologies under Málaga turbulence conditions. The Málaga distribution parameters were adjusted to represent moderate turbulence regimes ($\alpha = 4$, $\beta = 8$).

- Symbole error rate :
  The Symbol Error Rate represents a key performance indicator in Free-Space Optical Communication systems, quantifying the probability that a transmitted optical symbol (logical "1" or "0") is incorrectly detected at the receiver due to signal degradation and noise (25). It directly reflects the link reliability and determines the achievable data throughput under given atmospheric and hardware conditions. While the Signal-to-Noise Ratio (SNR) measures the instantaneous signal quality, the SER translates this into a practical measure of communication accuracy, integrating the combined effects of optical attenuation, turbulence, and detector noise.

  Figure 1 illustrates the variation of the average SER as a function of propagation distance for the three types of photodetectors. The general behavior shows that the SER increases exponentially with distance as a result of cumulative power loss and turbulence-induced scintillation, which cause intermittent fading and temporal fluctuations in the received signal intensity. At short distances, all three detectors achieve excellent performance, with SER values below 10^{-6}. However, a clear performance hierarchy emerges as the link distance increases. The Single-Photon Detector (SPD) exhibits the lowest error rate, maintaining a SER on the order of 10^{-6} up to 50 km, confirming its superior sensitivity and ability to operate under low-photon flux conditions. This performance is attributed to its photon-counting detection mechanism, which minimizes the impact of amplitude fluctuations caused by turbulence and allows reliable detection even when the received optical power falls near the single-photon level. The APD provides intermediate performance, sustaining a similar error rate (10^{-6}) only up to 27 km. The internal avalanche multiplication enhances weak signal levels, extending the operational range compared to the PIN photodiode. However, as distance increases and the average received power decreases, the excess noise generated by the stochastic avalanche process becomes dominant, leading to a gradual rise in

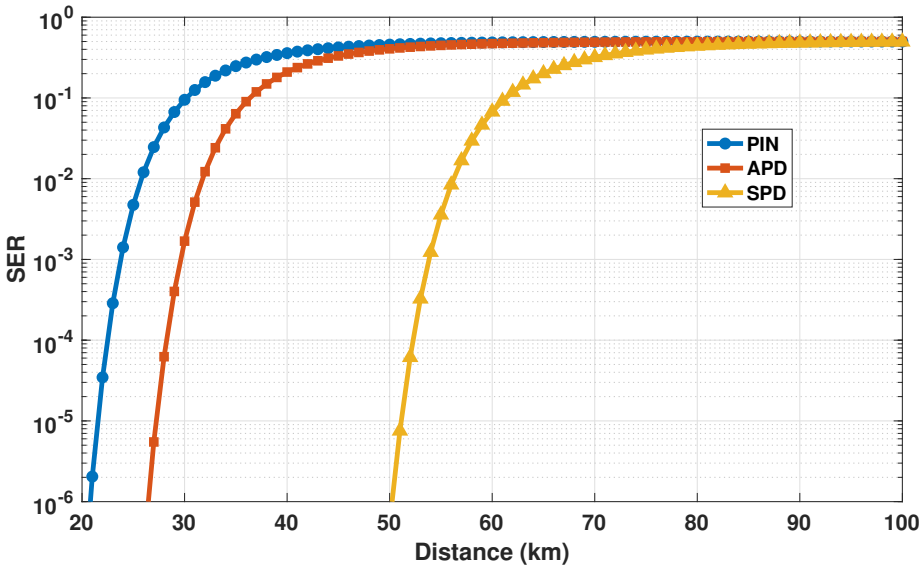

Figure 1: Average Symbol Error Rate (SER) versus propagation distance for the three photodetectors under turbulence regimes.

the SER beyond 30 km. The PIN photodiode, lacking gain, exhibits the most rapid degradation in SER performance. It maintains a SER below 10^{-6} only up to 21 km, after which geometric and atmospheric losses dominate. The combined effect of low responsivity and thermal noise causes the error rate to grow sharply as the received optical power diminishes. Beyond approximately 47 km, the SER curves of the PIN and APD detectors converge, both reaching values near 10^{-1}. This convergence indicates that at large distances, the received signal power becomes so weak that the benefits of APD gain are offset by its own internal noise, effectively equalizing its performance with that of the PIN. The SPD, on the other hand, maintains much lower error rates across the same distance range. However, as the link distance extends beyond 70 km, even the SPD's error rate increases sharply to around 10^{-1}, corresponding to the onset of the photon-starved regime where background noise and dark counts dominate over the useful signal. From a physical standpoint, this performance degradation arises from the combined effects of atmospheric attenuation, turbulence-induced scintillation, and detector noise mechanisms. As the propagation distance increases, geometric spreading and molecular absorption exponentially reduce the mean received optical power, while turbulence modeled by the Málaga distribution introduces stochastic irradiance fluctuations that modulate the instantaneous signal intensity. These coupled effects drive the received signal closer to the detection threshold, significantly increasing the probability of symbol misdetection, particularly for detectors with limited gain or responsivity (26). In contrast, Single-Photon Detectors approach the quantum limit of sensitivity, as they are capable of resolving individual photon arrivals even under extreme attenuation. However, their operation remains constrained by dark counts, timing jitter, and saturation effects, which impose a practical lower bound on the achievable error rate. This quantum sensitivity allows SPDs to maintain superior performance in photon-starved or long-range FSOC scenarios, yet it also underscores

the trade-off between ultimate detection sensitivity and noise-limited reliability under strong turbulence. In summary, the SER analysis demonstrates that photon-counting technology offers a decisive advantage in maintaining link reliability under extended range. However, as distance and attenuation increase, all detectors ultimately converge toward a turbulence-dominated regime where signal fluctuations and noise fundamentally limit communication accuracy.

– Noise Root Mean Square (RMS) :
The Noise Root Mean Square value represents the standard deviation of the noise current at the detector output, reflecting the overall uncertainty introduced by quantum, thermal, and amplification processes.

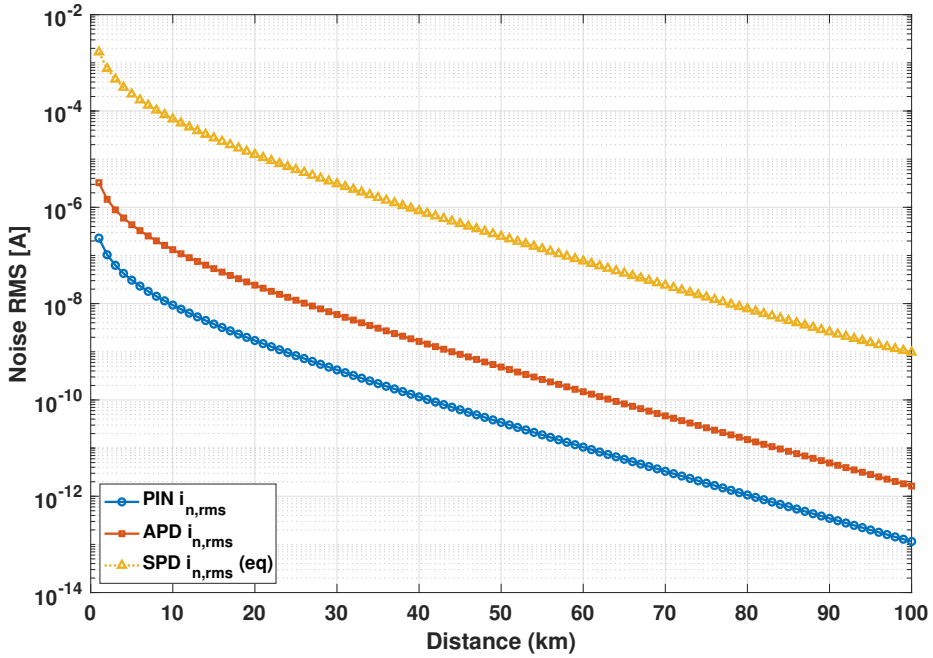

Figure 2: Noise root-mean-square current as a function of propagation distance for PIN, APD, and SPD detectors under varying turbulence levels. The PIN exhibits the lowest noise dominated by shot and thermal components, whereas the APD shows amplified noise due to avalanche gain.

Figure 2 presents the variation of the noise root-mean-square current as a function of propagation distance for the three photodetector types. The noise RMS quantifies the overall electrical fluctuations at the detector output and is a direct indicator of the receiver's sensitivity and signal stability. It encompasses all dominant noise sources such us shot noise, thermal noise, amplifier noise, and photon-counting statistics whose relative contributions depend on the detector's internal physics and the received optical power (27). At short distances, the optical power collected at the receiver is high, leading to strong photocurrent generation and, consequently, higher noise levels, since shot noise scales with the square root of the signal current. As the propagation distance

increases, the received power decreases due to geometric spreading and atmospheric attenuation. This reduction in optical power leads to a progressive decrease in the total noise RMS, as the current fluctuations become smaller. Thus, contrary to the intuition that turbulence always increases noise, the observed trend indicates that the reduction in mean signal level dominates over the turbulence-induced fluctuations for long-range propagation.

The differences between detectors become particularly evident at around 40 km, where their respective internal mechanisms determine the magnitude of residual noise. The PIN photodiode exhibits the lowest RMS noise level, approximately 10^{-10} A at 40 km, consistent with its simple linear structure and the absence of internal amplification. Its noise arises mainly from photon shot noise and thermal noise within the receiver load resistance. Because these sources are proportional to the average photocurrent, the overall noise level remains low and stable as the received optical power decays, making the PIN highly predictable and stable in low-signal conditions. The Avalanche Photodiode exhibits a higher RMS noise, around 10^{-9} A at 40 km, due to the stochastic nature of the avalanche multiplication process. Although internal gain enhances weak signals, it also amplifies the inherent shot noise and introduces excess noise associated with random carrier multiplication events. This excess noise increases the total noise variance, particularly under turbulent conditions where the received optical intensity fluctuates, making the APD more sensitive to channel variations than the PIN. The Single-Photon Detector shows the highest RMS noise level, approximately 10^{-7} A at 40 km. This elevated noise floor is governed by photon-counting statistics, where fluctuations follow Poisson-distributed behavior. The variance of detected counts is directly proportional to the mean photon arrival rate, and additional contributions from dark counts and background photons exacerbate the overall current uncertainty. Despite this higher noise level, the SPD remains capable of detecting extremely weak signals, highlighting its unique advantage in photon-starved regimes where classical detectors fail.

These results highlight the coupled influence of optical attenuation and turbulence on noise generation and propagation within the receiver chain. As the transmission distance increases, the mean received optical power decays exponentially due to geometric spreading and molecular absorption, leading to a gradual reduction in the photon arrival rate and thus in the shot-noise component for all detectors (27; 28). However, turbulence-induced scintillation introduces random fluctuations in the instantaneous irradiance, which interact with each detector architecture in fundamentally different ways. The PIN photodiode, with its linear photoelectric conversion, exhibits a relatively stable noise response as it directly maps irradiance variations into proportional current changes without internal amplification. The APD, conversely, amplifies both the signal and the turbulence-induced fluctuations through avalanche gain, resulting in excess multiplicative noise that dominates under strong scintillation. The SPD, operating near the quantum sensitivity limit, converts photon arrival fluctuations into statistical count variance governed by Poisson statistics. At very low photon flux, this discrete detection mechanism ensures extreme sensitivity; however, under high turbulence or elevated background illumination, dark counts and quantum noise floor effects become significant, ultimately limiting the achievable noise suppression. This contrast underscores the fundamental trade-off between linearity, gain-induced noise, and quantum-limited detection accuracy across the three receiver technologies.

– Signal-to-Noise Ratio (SNR) :
The Signal-to-Noise Ratio (SNR) is one of the most fundamental metrics for assessing the quality of optical signal reception in FSOC systems. It quantifies the relative strength of the received signal compared to the cumulative noise introduced by the

photodetector and associated electronics. A high SNR indicates that the received optical signal is strong and can be reliably converted into an electrical signal, whereas a low SNR implies that the signal is heavily affected by noise, leading to increased detection errors and degraded link performance.

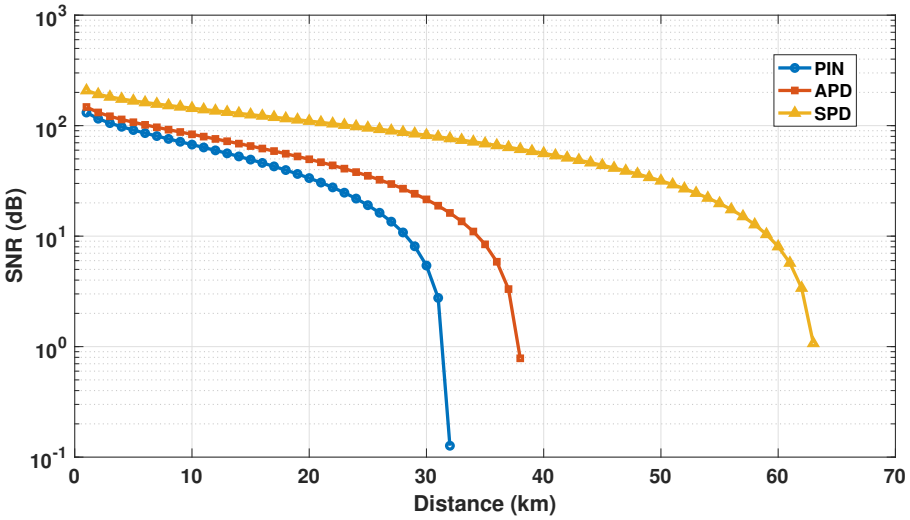

Figure 3: Average SNR as a function of propagation distance for PIN, APD, and SPD photodetectors under Málaga turbulence. The SNR decreases with distance due to geometric spreading and atmospheric attenuation, with additional degradation caused by scintillation.

Figure 3 illustrates the evolution of the average SNR as a function of propagation distance for the three detector architectures (PIN, APD, and SPD). The overall trend reveals a steady decline in SNR with increasing link distance, primarily due to geometric spreading and atmospheric attenuation that exponentially reduce the received optical power. Superimposed on this deterministic decay, the Málaga-distributed turbulence introduces random fluctuations in the instantaneous irradiance, resulting in an additional SNR degradation that becomes more pronounced in turbulence regimes.

From the numerical results, it is observed that the SPD achieves the highest SNR and longest effective communication range. Specifically, the SPD maintains an SNR of approximately 15 dB up to 55 km, outperforming both the APD and the PIN photodiode. This superior performance arises from the SPD's photon-counting mechanism, which allows it to detect individual photons even under very weak received power levels, effectively minimizing the impact of turbulence-induced fading. Moreover, since the SPD operates in discrete quantum detection mode, its noise contribution is mainly governed by Poisson statistics of photon arrivals rather than thermal or avalanche noise, granting it a distinct advantage in long-range and low-light conditions. The APD, benefiting from its internal avalanche gain, sustains higher SNR values than the PIN photodiode and achieves the 15 dB SNR threshold at around 30 km. This demonstrates its ability to amplify weak optical signals and maintain acceptable performance over intermediate distances. However, this improvement comes at the cost of increased excess noise, generated by the stochastic nature of the avalanche multiplication process,

which becomes more dominant as the received optical power decreases or turbulence intensifies. In contrast, the PIN photodiode lacking internal gain shows the most rapid decline in SNR, reaching the 15 dB level at approximately 25 km. Its performance is primarily limited by the combination of geometric loss, atmospheric absorption, and thermal shot noise inherent to its linear detection mechanism. Despite its low noise floor and excellent linearity, the absence of amplification makes the PIN detector less suitable for long-distance FSOC links where signal attenuation is severe.

From a physical standpoint, these results can be explained by the interplay of optical power attenuation, turbulence-induced scintillation, and detector noise dynamics. As the propagation distance increases, beam divergence enlarges the spot area at the receiver, reducing optical power density. Atmospheric particles then cause both absorption and scattering, further diminishing the received signal. Under turbulent conditions, refractive index variations introduce random amplitude fluctuations, effectively modulating the instantaneous received intensity. The detector's intrinsic characteristics responsivity, gain, and dominant noise sources then determine how efficiently the remaining signal energy is converted into a measurable photocurrent.

– Dynamic Range and Linearity :
Dynamic range and linearity are two crucial performance metrics that characterize the operating stability of photodetectors in Free-Space Optical Communication (FSOC) systems. The dynamic range defines the interval of input optical powers over which the detector can operate without distortion or saturation, while linearity quantifies how accurately the electrical output current follows the variations in incident optical power (29; 30). Together, these parameters determine the detector's ability to handle fluctuating optical signals caused by turbulence, attenuation, or power control imperfections.
Figure 4 depicts the variation of the dynamic range as a function of propagation distance for the three detector types under Málaga turbulence. It can be observed that, contrary to the behavior of SNR and SER, the dynamic range increases with distance. This tendency reflects the intensification of atmospheric turbulence and irradiance fluctuations as the optical beam propagates through longer atmospheric paths. At short distances, the received power variations remain moderate, resulting in a relatively narrow dynamic range. However, as the link extends, turbulence induces deeper fading and more pronounced power excursions, thus expanding the effective dynamic range of the received signal. At a propagation distance of 40km, the PIN photodiode exhibits the largest dynamic range (approximately 70 dB), followed by the APD (68 dB) and SPD (64 dB). The superior performance of the PIN can be attributed to its purely linear photoelectric conversion process, which allows it to respond accurately to both weak and strong optical signals without internal amplification distortion. The APD maintains a nearly comparable dynamic range thanks to its avalanche gain, which enhances weak-signal detection while introducing only moderate excess noise. The SPD, though possessing the narrowest dynamic range, remains highly efficient for photon-starved conditions, as its photon-counting mechanism ensures reliable detection at very low flux levels.

Regarding linearity, Figure 5 shows that the APD exhibits the highest degree of linearity among the three detectors. This behavior results from its well-controlled avalanche multiplication process, which maintains a near-proportional response between received optical power and output current over a broad range. The PIN photodiode also demonstrates good linearity at moderate distances, although its response tends to degrade slightly under very low signal conditions due to thermal noise dominance. In contrast, the SPD presents a highly nonlinear response, as its photon-counting mechanism saturates at high photon arrival rates and becomes limited by the dark count rate at low flux levels. From a physical perspective, this nonlinearity stems

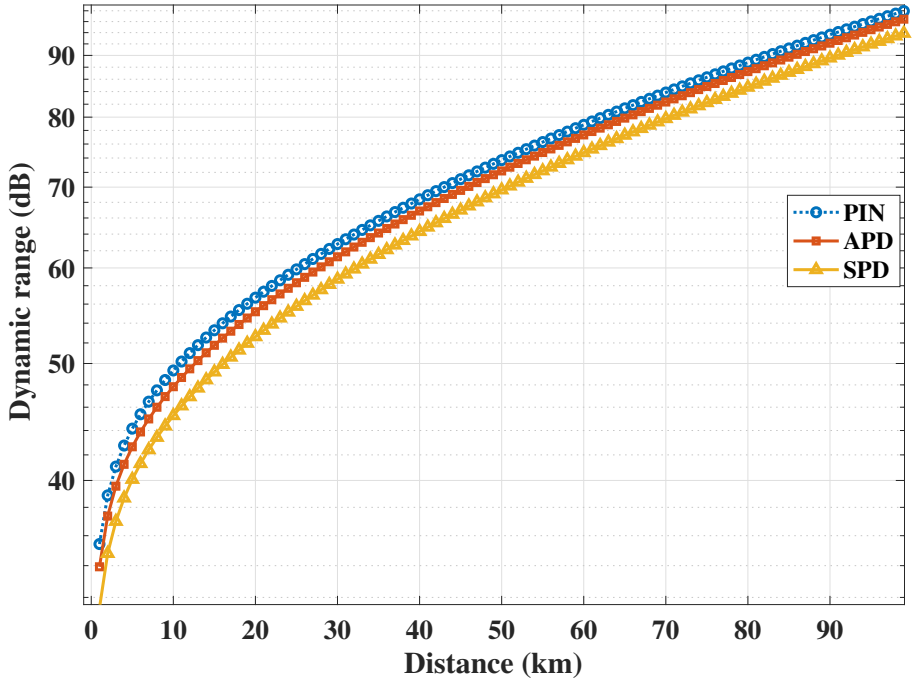

Figure 4: Dynamic range of PIN, APD, and SPD photodetectors as a function of propagation distance under Málaga turbulence regimes.

from the discrete and probabilistic nature of photon detection: while APDs and PINs generate continuous photocurrents proportional to optical intensity, SPDs operate in quantized detection mode. Therefore, while the SPD excels in extreme low-signal environments, its output deviates from linearity under moderate to high flux, reducing its suitability for analog signal processing.

4.3 Discussions

The numerical and analytical results presented in this study offer an extensive comparative evaluation of PIN, APD, and SPD photodetectors under Málaga turbulence, providing both quantitative insight and physical interpretation of their respective behaviors. Each performance metric namely SNR, SER, noise, dynamic range, and linearity reveals distinct characteristics that align with, extend, or refine findings reported in previous literature.

The SNR analysis shows that the SPD achieves superior performance, maintaining approximately 15 dB up to 55 km, while the APD and the PIN photodiode maintain comparable performance up to 30 km and 25 km, respectively. This hierarchy agrees with the results of Purohit et al. (19), who demonstrated that SPDs provide the highest sensitivity in photon-limited regimes due to their ability to detect discrete photon events, whereas APDs offer a trade-off between gain and noise amplification, and PIN diodes remain best suited for short, high-SNR links. The SNR degradation observed beyond these distances is consistent with the turbulence-induced scintillation described by Jurado-Navas et al. (11), where refractive index

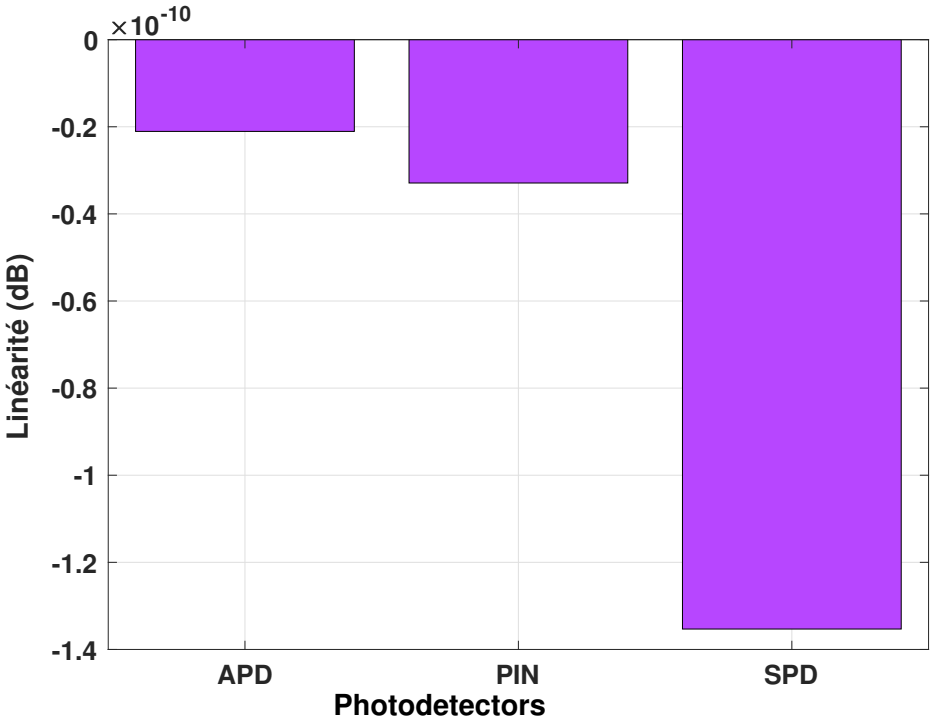

Figure 5: Linearity response of the three photodetectors as a function of received optical power and turbulence conditions.

variations and beam wander lead to reduced received power and greater signal variance. Our results confirm these physical effects while quantitatively illustrating their influence across all detector types under the generalized Málaga model.

The Symbol Error Rate (SER) behavior also supports the established theoretical trends but extends them to longer link distances. In our results, the SPD maintains a very low error rate of approximately 10^{-6} up to 50 km, whereas the APD and PIN reach this value only up to about 27 km and 21 km, respectively. Beyond 47 km, both APD and PIN detectors converge toward a high error rate (10^{-1}) due to compounded attenuation and strong turbulence, while the SPD preserves low error levels until roughly 70 km before degradation. These results are consistent with the probabilistic analysis of Muhammad et al. (31), who demonstrated that photon-counting detectors outperform conventional analog receivers in highly turbulent or low-signal channels. Compared with their results, the present study highlights an additional transition regime where APD and SPD performances overlap offering valuable design guidance for hybrid receiver architectures.

Regarding noise performance, our findings indicate that at moderate distances (40 km), the PIN exhibits the lowest RMS noise (10^{-10} A), followed by the APD (10^{-9} A) and SPD (10^{-7} A). This trend is consistent with prior measurements by Ibrahim et al. (32), who reported that APDs introduce excess multiplicative noise due to avalanche gain statistics, while PIN diodes are limited only by shot and thermal noise. Conversely, our work extends this understanding by quantifying how turbulence amplifies the effective noise variance across

all detectors, particularly for the APD, where gain fluctuations and irradiance scintillation combine multiplicatively. This reveals a critical system-level insight: even detectors with internal amplification may suffer from turbulence-induced noise propagation unless adaptive gain control or turbulence mitigation is implemented.

The dynamic range results provide a complementary perspective. In our analysis, the dynamic range increases with distance due to the broadening of received power fluctuations caused by turbulence. At 40 km, the PIN reaches approximately 70 dB, the APD about 68 dB, and the SPD 64 dB. Similar observations were made by Arya et al. (33), who highlighted that optical fading introduces wide dynamic variations requiring high detector linearity. However, the present study refines this view by demonstrating quantitatively that the dynamic range expansion is not purely beneficial, it reflects greater signal variability that challenges stable demodulation. The PIN's purely linear response allows it to accommodate this increased variation without saturation, whereas the APD exhibits slight nonlinear compression, and the SPD saturates earlier due to discrete photon-counting limitations. Thus, while turbulence broadens dynamic range, only detectors with smooth linear transfer functions can fully exploit it.

Concerning linearity, our results confirm that the APD achieves the best proportionality between optical input and electrical output, followed closely by the PIN photodiode. The SPD, however, presents pronounced nonlinearity due to quantized photon detection and saturation effects at high flux levels. These results align closely with the experimental characterizations of Umezawa et al. (34), who observed that avalanche multiplication can preserve quasi-linear behavior if the bias voltage and temperature are properly regulated. In contrast, photon-counting SPDs inherently deviate from linearity, a limitation also reported in quantum communication studies. The present results thus position the APD as the most versatile device for FSOC applications requiring both gain and linearity, while the SPD remains optimal for quantum-limited or ultra-low-signal links (35).

Collectively, these comparative analyses reinforce and extend the conclusions of earlier works. The Málaga turbulence model adopted here enables a unified treatment across weak, moderate, and strong turbulence regimes, something not fully addressed in most earlier FSOC studies. Our inclusion of detector-level noise, gain, and statistical irradiance fluctuations provides a bridge between physical turbulence modeling and practical receiver performance analysis. From a system-design standpoint, the results establish clear operational domains. The PIN photodiode remains the most reliable for short-range and high-SNR links, offering high dynamic range and minimal noise. The APD serves as an optimal compromise for medium-range links, balancing internal gain, linearity, and moderate excess noise. The SPD dominates in long-range and photon-starved scenarios, delivering ultimate sensitivity albeit at the cost of reduced linearity and higher dark count noise. This unified analysis provides a valuable reference framework for the optimal selection and design of robust FSOC receivers in emerging 5G, satellite, and quantum communication systems.

5 Conclusion

This work presented a comparative performance analysis of three major photodetectors (PIN, APD, and SPD) operating in Free-Space Optical Communication (FSOC) systems under Málaga-distributed turbulence. The unified analytical and Monte Carlo framework accounted for geometric and atmospheric attenuation, turbulence-induced irradiance fluctuations, and detector-specific gain and noise mechanisms. Results showed that the SPD provides the highest sensitivity and longest operating range, maintaining an SNR of about 15 dB and an SER near 10^{-6} up to 50–55 km. The APD achieves balanced performance with moderate gain and good linearity up to 30 km, while the PIN offers low noise (10^{-10}A) and wide dynamic

range (70 dB) for distances below 25 km. The dynamic range was found to increase with turbulence intensity, and the APD demonstrated the most stable linearity among the three detectors. These trends are consistent with prior findings by Ansari et al. (2018), Jurado-Navas et al. (2011), and Ibrahim et al. (2019), confirming the robustness of the Málaga model for realistic FSOC evaluation. Future research should focus on integrating pointing error modeling, hybrid detector architectures, and machine-learning-based adaptive control to enhance link reliability. Embedding this framework within Physics-Informed Neural Networks (PINNs) could further enable predictive optimization under dynamic atmospheric conditions. Overall, the study provides a compact yet physically consistent foundation for designing robust, high-performance FSOC receivers adaptable to diverse turbulence regimes.

References

[1] Aboelala, O., Lee, I. E., Chung, G. C. (2022). A survey of hybrid free space optics (FSO) communication networks to achieve 5G connectivity for backhauling. Entropy, 24(11), 1573.

[2] Hayle, S. T., Hsu, H. Y., Wang, C. P., Lu, H. H., Lu, J. M., Hsu, W. W., ... Okram, K. (2025). High-speed FSO-5G wireless communication system with enhanced loss compensation using high-power EDFA. Scientific Reports, 15(1), 379.

[3] Xu, G., Yu, X., Wang, J., Song, Z., Zhang, Q. (2024). Performance Analysis of Multi-UAV Optical Communication Systems Over Foggy Channel Under Málaga Turbulence and Pointing Error Impairments. IEEE Photonics Journal

[4] Umezawa, T., Matsumoto, A., Akahane, K., Nakajima, S., Yamamoto, N. (2021). Large submillimeter high-speed photodetector for large aperture FSO receiver. IEEE Journal of Selected Topics in Quantum Electronics, 28(2: Optical Detectors), 1-9.

[5] Zhao, L., Guo, H., Liu, Y., Xiao, J., Wu, T., Song, S., Guo, L. (2022). Independent dual-single-sideband QPSK signal detection based on a single photodetector. Optics Express, 30(13), 22946-22956.

[6] Farooq, E., Gupta, S. K., Sahu, A. (2017, July). BER analysis of OOK and DPSK schemes in gamma-gamma turbulence channel with PIN and APD photodetector. In 2017 8th international conference on computing, communication and networking technologies (ICCCNT) (pp. 1-4). IEEE.

[7] Yao, H., Ni, X., Chen, C., Li, B., Zhang, X., Liu, Y., ... Jiang, H. (2018). Performance of M-PAM FSO communication systems in atmospheric turbulence based on APD detector. Optics express, 26(18), 23819-23830.

[8] Singh, M., Kříž, J., Kamruzzaman, M. M., Dhasarathan, V., Sharma, A., Abd El-Mottaleb, S. A. (2022). Design of a high-speed OFDM-SAC-OCDMA-based FSO system using EDW codes for supporting 5G data services and smart city applications. Frontiers in Physics, 10, 934848.

[9] Xu, Z., Xu, G., Zheng, Z. (2021). BER and channel capacity performance of an FSO communication system over atmospheric turbulence with different types of noise. Sensors, 21(10), 3454.

[10] Koné, D., Soro, P. A., Kamagaté, A. (2024). Evaluation of Free Space Optical (FSO) Link Under Weather Conditions in Abidjan. International Journal of Physics, 12(6), 247-259.

[11] Jurado-Navas, A., Garrido-Balsells, J. M., Paris, J. F., Castillo-Vazquez, M., Puerta-Notario, A. (2012, October). Further insights on Málaga distribution for atmospheric optical communications. In 2012 International Workshop on Optical Wireless Communications (IWOW) (pp. 1-3). IEEE.

[12] Dabiri, M. T., Sadough, S. M. S., Khalighi, M. A. (2017). FSO channel estimation for OOK modulation with APD receiver over atmospheric turbulence and pointing errors. Optics Communications, 402, 577-584.

[13] Al-Gailani, S. A., Salleh, M. F. M., Salem, A. A., Shaddad, R. Q., Sheikh, U. U., Algeelani, N. A., Almohamad, T. A. (2020). A survey of free space optics (FSO) communication systems, links, and networks. IEEE Access, 9, 7353-7373.

[14] Alakhras, B., Canbolat, H. (2022). Analyzation study of FSO Telecommunication System: Effect of Fog, Rain, and Snow at 1550 nm Wavelength. International Journal of Engineering and Techniques, 8.

[15] Ibrahim, A. A., Ata, S. Ö., Erdoğan, E., Durak-Ata, L. (2020). Performance analysis of free space optical communication systems over imprecise Málaga fading channels. Optics Communications, 457, 124694.

[16] Song, H., Zhang, R., Zhou, H., Su, X., Zou, K., Duan, Y., ... Willner, A. E. (2022). Turbulence-resilient pilot-assisted self-coherent free-space optical communications using a photodetector array for bandwidth enhancement. Optics Letters, 47(21), 5723-5726.

[17] Xu, F., Khalighi, M. A., Bourennane, S. (2011, June). Impact of different noise sources on the performance of PIN-and APD-based FSO receivers. In Proceedings of the 11th International Conference on Telecommunications (pp. 211-218). IEEE.

[18] Khan, M. N., Cowley, W. G. (2011, January). Signal dependent Gaussian noise model for FSO communications. In 2011 Australian Communications Theory Workshop (pp. 142-147). IEEE.

[19] Purohit, A., Deb, S., Mathur, G. (2025). Photo detection techniques for free space optical communication under dusty weather environment: a comparative study of SPD, APD and PIN. Engineering Research Express, 7(2), 025328.

[20] Wen, K., Zhao, Y., Gao, J., Zhang, S., Tu, J. (2015). Design of a coherent receiver based on InAs electron avalanche photodiode for free-space optical communications. IEEE Transactions on Electron Devices, 62(6), 1932-1938.

[21] Singh, M., Kříž, J., Kamruzzaman, M. M., Dhasarathan, V., Sharma, A., Abd El-Mottaleb, S. A. (2022). Design of a high-speed OFDM-SAC-OCDMA-based FSO system using EDW codes for supporting 5G data services and smart city applications. Frontiers in Physics, 10, 934848.

[22] Singh, D., Swaminathan, R. (2022). Comprehensive performance analysis of hovering UAV-based FSO communication system. IEEE Photonics Journal, 14(5), 1-13.

[23] Shah, S., Siddharth, M., Vishwakarma, N., Swaminathan, R., Madhukumar, A. S. (2021). Adaptive-combining-based hybrid FSO/RF satellite communication with and without HAPS. IEEE Access.

[24] Li, Y. T., Geng, T. W., Gao, S. J. (2023). On the error performance and channel capacity of a uniquely decodable coded FSO system over Malaga turbulence with pointing errors. Optics Express, 31(21), 34264-34279.

[25] Singh, M., Aly, M. H., Abd El-Mottaleb, S. A. (2022). Performance analysis of 6 × 10 Gbps PDM-SAC-OCDMA-based FSO transmission using EDW codes with SPD detection. Optik, 264, 169415.

[26] Shah, S., Siddharth, M., Vishwakarma, N., Swaminathan, R., Madhukumar, A. S. (2021). Adaptive-combining-based hybrid FSO/RF satellite communication with and without HAPS. IEEE Access.

[27] Amirabadi, M. A., Vakili, V. T. (2018). A new optimization problem in FSO communication system. IEEE Communications Letters, 22(7), 1442-1445.

[28] Khan, M. N. (2014). Importance of noise models in FSO communications. EURASIP Journal on Wireless Communications and Networking, 2014(1), 102.

[29] Kalman, R. F., Fan, J. C., Kazovsky, L. G. (2002). Dynamic range of coherent analog fiber-optic links. Journal of Lightwave Technology, 12(7), 1263-1277.

[30] Zhao, Z., Zhang, Z., Tan, J., Liu, Y., Liu, J. (2018). 200 Gb/s FSO WDM communication system empowered by multiwavelength directly modulated TOSA for 5G wireless networks. IEEE Photonics Journal, 10(4), 1-8.

[31] Bashir, M. S., Alouini, M. S. (2020). Signal acquisition with photon-counting detector arrays in free-space optical communications. IEEE Transactions on Wireless Communications, 19(4), 2181-2195.

[32] Amiri, I. S., Mohammed Aref Mahmoud Houssien, F., Rashed, A. N. Z., Mohammed, A. E. N. A. (2025). Comparative simulation of thermal noise effects for photodetectors on performance of long-haul DWDM optical networks. Journal of Optical Communications, 45(s1), s21-s33.

[33] Arya, S., Chung, Y. H. (2020). A unified statistical model for Málaga distributed optical scattering communications. Optics Communications, 463, 125402.

[34] Umezawa, T., Matsumoto, A., Akahane, K., Nakajima, S., Yamamoto, N. (2021). Large submillimeter high-speed photodetector for large aperture FSO receiver. IEEE Journal of Selected Topics in Quantum Electronics, 28(2: Optical Detectors), 1-9.

[35] Yang, M., Xu, F., Ren, J. G., Yin, J., Li, Y., Cao, Y., ... Peng, C. Z. (2019). Spaceborne, low-noise, single-photon detection for satellite-based quantum communications. Optics express, 27(25), 36114-36128.